Observational Constraints on the Oxidation of NO_x in the Upper Troposphere

Benjamin. A. Nault,[†] Charity Garland,[‡] Paul J. Wooldridge,[‡] William H. Brune,[‖] Pedro Campuzano-Jost,[⊥] John D. Crounse,[#] Douglas A. Day,[⊥] Jack Dibb,[▽] Samuel R. Hall,[¶] L. Gregory Huey,[£] José L. Jimenez,[⊥] Xiaoxi Liu,[£] Jingqiu Mao,[$] Tomas Mikoviny,[&] Jeff Peischl,[^] Ilana B. Pollack,[^,%] Xinrong Ren,[+] Thomas B. Ryerson,[^] Eric Scheuer,[▽] Kirk Ullmann,[¶] Paul O. Wennberg,[┤] Armin Wisthaler,[=] Li Zhang,[‖] Ronald C. Cohen[†,‡,*]

[†]Department of Earth and Planetary Science, University of California, Berkeley, California 94709, United States

[‡]Department of Chemistry, University of California, Berkeley, California 94709, United States

[‖]Department of Meteorology, Pennsylvania State University, University Park, Pennsylvania 16802, United States

[⊥]Cooperative Institute for Research in the Environmental Sciences and Department of Chemistry and Biochemistry, University of Colorado, Boulder, Colorado 80309, United States

[#]Division of Chemistry and Chemical Engineering, California Institute of Technology, Pasadena, California 91125, United States

[▽]Earth Systems Research Center, Institute for the Study of Earth Oceans and Space, University of New Hampshire, Durham, New Hampshire 03824, United States

[¶]Atmospheric Chemistry Division, National Center for Atmospheric Research (NCAR), Boulder, Colorado 80307, United States

[£]School of Earth and Atmospheric Sciences, Georgia Institute of Technology, Atlanta, Georgia 30332, United States

[$]National Oceanic and Atmospheric Administration Geophyiscal Fluid Dynamics Laboratory, Princeton, New Jersey 08540, United States

[&]Oak Ridge Associated Universities, Oak Ridge, Tennessee 37831, United States

[^]Chemical Sciences Division, Earth System Research Lab, National Oceanic and Atmospheric Administration, Boulder, Colorado 80305, United States

[%]Now at: Atmospheric Science Department, Colorado State University, Fort Collins, Colorado 80523, United States

[+]Air Resources Laboratory, National Oceanic and Atmospheric Administration, College Park, Maryland 20740, United States

[┤]Division of Engineering and Applied Science and Division of Geological and Planetary Sciences, California Institute of Technology, Pasadena, California 91125, United States

[═]Institute of Ion Physics and Applied Physics, University of Innsbruck, Innsbruck, Austria

Corresponding Author

[*]Phone: (510)-642-2735. E-mail: rccohen@berkeley.edu

Abstract

NO_x ($NO_x \equiv NO + NO_2$) regulates O_3 and HO_x ($HO_x \equiv OH + HO_2$) concentrations in the upper troposphere. In the laboratory, it is difficult to measure rates and branching ratios of the chemical reactions affecting NO_x at the low temperatures and pressures characteristic of the upper troposphere, making direct measurements in the atmosphere especially useful. We report quasi-Lagrangian observations of the chemical evolution of an air parcel following a lightning event that results in high NO_x concentrations. These quasi-Lagrangian measurements obtained during the Deep Convective Clouds and Chemistry experiment are used to characterize the daytime rates for conversion of NO_x to different peroxy nitrates, the sum of alkyl and multifunctional nitrates, and HNO_3. We infer the following production rate constants (in cm^3/molecules/s) at 225 K and 230 hPa: $7.2(\pm5.7)\times10^{-12}$ ($CH_3O_2NO_2$), $5.1(\pm3.1)\times10^{-13}$ (HO_2NO_2), $1.3(\pm0.8)\times10^{-11}$ (PAN), $7.3(\pm3.4)\times10^{-12}$ (PPN), and $6.2(\pm2.9)\times10^{-12}$ (HNO_3). The HNO_3 and HO_2NO_2 rates are ~30 – 50% lower than currently recommended while the other rates are consistent with current recommendations to within ±30%. The analysis indicates that HNO_3 production from the HO_2 and NO reaction (if any) must be accompanied by a slower rate for the reaction of OH with NO_2, keeping the total combined rate for the two processes at the rate reported for HNO_3 production above.

1. Introduction

In the upper troposphere, where O_3 is an important greenhouse gas,[1] NO_x ($NO_x \equiv NO + NO_2$) regulates O_3 production. NO_x concentrations in this region of the atmosphere are affected by transport including import from the stratosphere, convection, and large-scale descent, emissions from aircraft, *in-situ* production by lightning, and photochemical reactions that convert NO_x to higher oxides, or NO_z (Figure 1).[2-5] The higher oxides include HNO_3 (R1a and R2b), alkyl and multifunctional nitrates (R3b), and acyl and non-acyl peroxy nitrates (R4 and R5).

$$NO_2 + OH + M \xrightarrow{k_{1a}} HNO_3 + M$$

(R1a)

$$NO_2 + OH + M \xrightarrow{k_{1b}} HOONO + M$$

(R1b)

$$HOONO + M \xrightarrow{k_{-1b}} NO_2 + OH + M$$

(R−1b)

$$NO + HO_2 \xrightarrow{k_{2a}} NO_2 + OH$$

(R2a)

$$NO + HO_2 \xrightarrow{k_{2b}} HNO_3$$

(R2b)

$$NO + RO_2^{\bullet} \xrightarrow{k_{3a}} NO_2 + RO^{\bullet}$$

(R3a)

$$NO + RO_2^{\bullet} \xrightarrow{k_{3b}} RONO_2$$ (R3b)

$$NO_2 + R(O)O_2^{\bullet} + M \xrightarrow{k_4} R(O)O_2NO_2 + M$$

(R4)

$$R(O)O_2NO_2 + M \xrightarrow{k_{-4}} NO_2 + R(O)O_2^{\bullet} + M$$

(R−4)

$$NO_2 + RO_2^{\bullet}\left(HO_2^{\bullet}\right) + M \xrightarrow{k_5} RO_2NO_2\left(HO_2NO_2\right) + M$$

(R5)

$$RO_2NO_2\left(HO_2NO_2\right) + M \xrightarrow{k_{-5}} NO_2 + RO_2^{\bullet}\left(HO_2^{\bullet}\right) + M$$

(R−5)

It has been typically assumed (with support from calculations) that production of HNO_3 strongly regulates the upper tropospheric NO_x lifetime with other NO_z playing a minor role.[6-8] However, there are relatively few laboratory studies constraining the rate constants for the production of NO_z under the conditions of the upper troposphere (T less than 250 K and P less than 400 hPa). For example, there are no laboratory observations of the rate constants for production of peroxy acetyl nitrate (PAN) and proxy propionyl nitrate (PPN) at temperatures less than 240 K.

The main sink of NO_x, formation of HNO_3, has been subject of the most laboratory experiments. Total loss of OH in the reaction of OH with NO_2 is known to represent production of HNO_3 (R1a) and peroxynitrous acid (HOONO, R1b).[9] The production of HOONO has only been studied at room temperature,[9] where the branching is 87% to HNO_3 and 13% to HOONO. Significant extrapolations are involved at the temperatures and pressures of the upper troposphere. Estimates of the branching are 75% for HNO_3 and 25% for HOONO at T = 225 K

and P = 230 hPa.[10] In addition to R1a, some laboratory studies[11-13] have measured the yield of HNO_3 from the reaction of HO_2 and NO (R2b) and suggest that this minor branch has non-zero yield of less than 1%. Since the overall rate of HO_2 and NO is of order 10 – 100 times faster than the OH and NO_2 reaction in the atmosphere, this low yield, if correct, represents an important sink of NO_x and source of HNO_3. Laboratory measurements of yields in this range are extremely difficult as secondary reactions (e.g., R2a then R1a) in the gas phase or on the walls of the reaction vessel can be significant interferences.

Other sinks of NO_x are also important in the upper troposphere. For example, pernitric acid (HO_2NO_2) and methyl peroxy nitrate ($CH_3O_2NO_2$) are important short-lived NO_x reservoirs—less than 24 hours through thermal decomposition (R4), photolysis (R6), or reaction of HO_2NO_2 with OH (R7). For the conditions of the upper troposphere, several studies of the rate of HO_2 with NO_2 are available[14-17] and one study for the rate of CH_3O_2 with NO_2[18] is available. Bacak et al.[14] report that the HO_2NO_2 production rate is almost 50% slower than currently recommended[10] and observed in prior experiments.[15-17]

$$RO_2NO_2\left(HO_2NO_2\right) + h\nu \xrightarrow{k_{6a}} NO_2 + RO_2^{\bullet}\left(HO_2^{\bullet}\right) \quad \text{(R6a)}$$

$$RO_2NO_2\left(HO_2NO_2\right) + h\nu \xrightarrow{k_{6b}} NO_3 + RO^{\bullet}\left(HO^{\bullet}\right) \quad \text{(R6b)}$$

$$HO_2NO_2 + OH \xrightarrow{k_7} NO_2 + O_2 + H_2O \quad \text{(R7)}$$

Any increases in the upper tropospheric NO_x lifetime will lead to increases in O_3 concentration.[14,19] This leads to higher O_3 radiative impacts. Recently, Romps et al.[20] described an

analysis of lightning that predicts its increase in a warmer climate. The additional NO_x associated with lightning will result in higher O_3 than today in the upper troposphere and increases in its radiative forcing; thus, it is important to understand NO_x lifetime in the upper troposphere.

To investigate the rates of NO_x oxidation, we analyze a quasi-Lagrangian experiment that observed the temporal evolution of NO, NO_2, $CH_3O_2NO_2$, HO_2NO_2, PAN, PPN, the sum of alkyl and multifunctional nitrates, HNO_3, and submircron aerosol nitrate downwind of a lightning storm on June 21st, 2012. The observations were obtained during the Deep Convective Clouds and Chemistry (DC3) experiment.[21] To assess the impacts of rate coefficients we derive on the chemistry of NO_x in the upper troposphere, we use a global chemical transport model to compare O_3, OH, HO_2, and NO_x for standard chemistry and the modified set of rate constants.

2. Instrumentation

The observations described here were made aboard the NASA DC-8 during the DC3 experiment (May − June, 2012).[21] All data used in this study can be accessed through the NASA public archives for this mission.[22] We use the Version 5 60 s merged files.

NO_2 was measured by the UC Berkeley thermal-dissociation laser-induced fluorescence (TD-LIF) instrument.[23] Briefly, a tunable dye laser pumped at 7 kHz by a Q-switched, frequency doubled Nd:YAG laser, produces ~20 ns pulses at 585 nm with a bandwidth of 0.06 cm^{-1}. The dye laser is tuned onto (9 s) and off (3 s) an isolated rovibronic feature of the jet-cooled[24] NO_2 at 585 nm. The difference between the two signals is directly proportional to the NO_2 mixing ratios. At the pressures of this flight (230 hPa), the ratio of the resonant peak to the non-resonant background fluorescence is 10 to 1. The laser light is focused through two multi-pass White

cells. The red-shifted fluorescence from the excited NO_2 molecules is detected using a red-sensitive photomultiplier tube (Hamamatsu H7421-50). Scattered light is removed using time gated detection and dielectric band pass filters that block light at wavelengths shorter than 700 nm. The instrument is calibrated at least every hour during a level flight leg or after a significant change in altitude using a 4.67 (±0.26) ppmv NO_2 standard (Praxair) diluted to ~ 2 – 8 ppbv in zero air. The accuracy and stability of the reference is compared against a library of other NO_2 standards in our laboratory on a regular basis. Fluorescence quenching by water vapor is accounted for[23] using the diode laser hygrometer (DLH) measurements of H_2O.[25] Partial thermal decomposition of $CH_3O_2NO_2$ in the NO_2 sample[26] is corrected by concurrent measurements of $CH_3O_2NO_2$ using thermal-dissociation with laser-induced fluorescence detection of the NO_2 enhancement.[27] During this flight, the maximum correction to the NO_2 measurements due to thermal decomposition of $CH_3O_2NO_2$ is 10% with a median correction of 7% for the entire flight. The correction is described in Nault et al.[27]

The measurements of $CH_3O_2NO_2$, sum of all peroxy nitrates (ΣPNs = PAN + PPN + HO_2NO_2 + $CH_3O_2NO_2$), and sum of alkyl and multifunctional nitrates in the gas- and particle-phase ($\Sigma ANs_{(g+p)}$ = all molecules of the chemical form $RONO_2$) have been described elsewhere[27-30] and the specific configuration during DC3 by Nault et al.[27] Briefly, the $CH_3O_2NO_2$, ΣPNs, and $\Sigma ANs_{(g+p)}$ are detected by thermal conversion to NO_2 in heated quartz tubes (60°C, 200°C, and 400°C, respectively) and detected by laser-induced fluorescence of the NO_2 fragment. The concentrations of $CH_3O_2NO_2$ and ΣPNs are calculated from the difference in the signal between the ambient NO_2 measurements and the 60°C and 200°C channel, respectively. Similarly, the concentrations of $\Sigma ANs_{(g+p)}$ are calculated from the difference in the signal between the 200°C and 400°C channel.

The temperature selected for the thermal decomposition (60°C) of $CH_3O_2NO_2$ was selected to minimize the amount of HO_2NO_2 that thermally decomposed. At that temperature and with a residence time of 0.08 s, we calculated that ~10% of HO_2NO_2 thermally decomposes.[27] The $CH_3O_2NO_2$ measurements are corrected using HO_2NO_2 observed by chemical ionization-mass spectrometry (CIMS)[33] as described by Nault et al.[27] The maximum correction is 10% with a median correction of 5% for the entire flight. Our estimates indicate that no other peroxy nitrates have important effects on the $CH_3O_2NO_2$ and $\sum$PNs measurements.[27]

In addition to the NO_2, $CH_3O_2NO_2$, ΣPNs, and $\Sigma ANs_{(g+p)}$ measurements, we use the measurements of NO and O_3 by chemiluminescence,[34] OH and HO_2 by laser-induced fluorescence,[35] gas-phase nitric acid ($HNO_{3,g}$), CH_3OOH, $CH_3C(O)OOH$, and hydroxyacetone by chemical ionization-mass spectrometry (CIMS),[36,37] particle-phase inorganic nitrate (NO_3^-) and particulate organic nitrate ($\Sigma ANs_{(p)}$) by aerosol mass spectrometry (AMS),[38,39] the sum of gas- and particle-phase nitric acid ($HNO_{3(g+p)}$) by mist chamber-ion chromatography (IC),[40] hydrocarbons (i.e., ethane, propane, ethene, n-butane) by whole air sampling with gas-chromatography analsysis,[41] PAN, PPN, and HO_2NO_2 by chemical ionization-mass spectrometry,[33,42] methyl vinyl ketone (MVK), methacrolein (MACR), acetone, acetaldehyde, isoprene, benzene, toluene, C10 terpenes (i.e., α-pinene) and C8 aromatics (i.e., m-xylene) by proton transfer reaction-mass spectrometry,[43] and CH_4 by tunable diode laser absorption spectroscopy,[25,44] (Table 1). Here, $HNO_{3(g+p)}$ is taken as the average of the CIMS and IC measurements. An intercomparison and treatment of the HO_2NO_2, peroxy nitrates, and $HNO_{3,(g+p)}$ measurements are described in the Supporting Information. Also, an intercomparison of photostationary steady state NO_2 versus measured NO_2 is described in the Supporting Information.

3. Results

On 21 June 2012, the NASA DC-8 sampled the photochemistry of a decaying mesoscale convective system over the central United States (Fig. 2) at a near constant temperature and pressure of 225 K and 230 hPa (~7.3×10^{18} molecules/cm^3). The decaying mesoscale convective system and flight are described in Barth et al.[21] Briefly, the DC-8 flew 5 legs spaced at varied distances downwind of the convection (full flight Fig. S3). Portions of the last three legs that we characterize as sampling the outflow in a quasi-Lagrangian sense are shown in Fig. 2, along with our estimate of the location of the cloud outflow marked as the green dashed-dot line. We define time zero as the first point in our sampling at 13:35 UTC. We estimate this was less than 10 minutes after the air left the cloud. The observations used in our analysis are those that are in the portions of the flight track that were approximately perpendicular to the flow. As the outflow was a line source, all points sampled can be thought of as having a common chemical origin and time evolution. The specific data we use are measurements initialized at 13:35 UTC (7:35 local time) and continuing to 8100 s after the initial time (15:50 UTC). . Using the distance between the legs (~50 and 100 km) and the wind speed (~25 m/s), we calculate that it takes the air ~2000 s to travel from a point in leg 1 to 2 and 4000 s from a point in leg 2 to 3, respectively. Based on this calculation, the observation time (relative to 13:35 UTC) and the transit time form that point are approximately equal, and we define the observation time difference as the time that the air parcel has evolved in the subsequent analysis.

Initializing the observations at the point observed at 13:35 UTC, we observed a decay in NO_x and production of $CH_3O_2NO_2$, HO_2NO_2, PAN, PPN, ΣPNs_i, $\Sigma ANs_{(g+p)}$, and $HNO_{3(g+p)}$ (Fig. 3

and S4). NO and NO_2 decayed by 190(±70) and 90(±20) pptv from an initial median mixing ratio of 670 and 270 pptv, respectively. The uncertainty in the decay represents the inter-quartile of the change. This corresponds to a total loss rate of $2.6(\pm0.6)\times10^5$ molecules/cm^3/s, if we assume chemical loss of NO_x is constant and linear over the 8000 s between the initial and final observation. Over the same interval, the production of the four peroxy nitrates was 140(±25) ($CH_3O_2NO_2$), 20(±5) (HO_2NO_2), 15(±5) (PAN), and 5(±1) (PPN) pptv. The initial median mixing ratios for the four peroxy nitrates was 0 ($CH_3O_2NO_2$), 50 (HO_2NO_2), 210 (PAN), and 20 (PPN) pptv. The $\Sigma ANs_{(g+p)}$ concentration grew 45(±20) pptv, from an initial 105 pptv, or $4.1(\pm1.8)\times10^4$ molecules/cm^3/s, while $\sum ANs_{(p)}$ increased by 7(±2) pptv, from an initial 5 pptv. Finally, $HNO_{3,(g+p)}$ increased by 40(±5) pptv, from an initial 38 pptv, or $3.6(\pm0.5)\times10^4$ molecules/cm^3/s. The loss rate of NO_x is, within the measurement uncertainty, identical to the production rate of the higher oxide species ($2.3(\pm0.3)\times10^5$ molecules/cm^3/s), indicating the observations of the decay of NO_x are consistent with the formation of NO_z.

Analysis of observations of ethene, ethyne, and toluene confirm the air mass is evolving in isolation with little mixing. These three hydrocarbons are selected since their only known source in the upper troposphere is convection.[45,46] OH was constant to within 25% in this segment of the flight at 9.5×10^6 molecules/cm^3. The OH concentration stayed constant during this time since its sources (e.g., CH_2O) and sinks (e.g., NO_x) decayed at similar rates. Using the measured decay of ethene—initial median mixing ratio of 43 pptv and final median mixing ratio of 14 pptv—and this OH concentration, we find a value of $1.0(\pm0.4)\times10^{-11}$ cm^3/molecules/s (Fig. 4) for the rate constant for the reaction of ethene with OH. The 2σ uncertainty of 40% is determined by adding the uncertainty of the slope (±7%) and the uncertainty of the OH measurement ($1\sigma \approx 16\%$) in quadrature. This is nearly identical to the recommended rate

constant of $8.9^{+2.1}_{-1.9}\times10^{-12}$ cm^3/molecules/s at 225 K and 230 hPa.[10] Doing a similar analysis with the decay of ethyne (initial and final median values of 98 to 89 pptv, respectively) and toluene (initial and final median values of 25 pptv to 14 pptv, respectively), we find values of $6.3(\pm3.5)\times10^{-13}$ and $1.1(\pm0.4)\times10^{-11}$ cm^3/molecules/s (Fig. S5), respectively. These ethyne and toluene rate constants are also nearly identical to the recommended rate constants of $7.0^{+1.1}_{-1.0}\times10^{-13}$ and $8.8^{+8.2}_{-4.3}\times10^{-12}$ cm^3/molecules/s, respectively.[10,47] The 2σ is calculated the same as for the ethene rate constant. In addition to confirming the air parcel is evolving in isolation, the ability to calculate these three rate constants within the uncertainty of the recommended values support the combined assumptions made about the evolution of the air parcel as a quasi-Lagrangian air parcel for 8000 s. If we assume the uncertainty in the slopes of the calculations is largely driven by uncertainty in the elapsed time, then the uncertainty in time is 10 – 40%. However, other uncertainties likely contribute, indicating a smaller range for the uncertainty in reaction time is more likely. In conclusion, the analysis of the hydrocarbon decay confirms that the initial observations (t = 0) occurred at 13:35 UTC and confirms our time coordinates as time in seconds since 13:35 UTC.

4. Analysis

4.1 Nitric acid production

We apply the same assumptions to analysis of the rate of oxidation of NO_x, starting with an analysis of $HNO_{3,(g+p)}$ production. The $HNO_{3,(g+p)}$ production rate, $dHNO_{3,(p+g)}/dt$, is calculated by subtracting the initial $HNO_{3,(g+p)}$ concentrations at time 0, which is 2.8×10^8 molecules/cm^3 at 13:35 UTC, from $HNO_{3,(g+p)}$ concentrations at time t. We use small time increments to account

for other processes affecting the NO_2 available for reaction (R4 – R5 and photolysis). The measured $dHNO_{3,(g+p)}/dt$ is plotted versus the corresponding NO_2 concentration at that time, t (Fig. 5). Similar to the hydrocarbon rate constant calculation (Sect. 3), we assume any uncertainty in the time after the initial observation is incorporated in the uncertainty of the slope. We find that the rate constant is $6.2(\pm2.9)\times10^{-12}$ cm^3/molecules/s, with the 2σ uncertainty defined as for ethene. This rate constant (T = 225 K and P = 230 hPa) is slower than recommended by Atkinson et al.[31] and Sander et al.[10] and nearly identical to the recommendation of Henderson et al.,[48] who derived a slower rate based on observations of NO_x and HNO_3 concentrations in the upper troposphere during the Intercontinental Chemical Transport Experiment – North America (Fig. 6).

Given that the standard k_{1a} rate constant alone results in more rapid production of HNO_3 than we observe, it is straightforward to conclude that any additional production from the reaction of HO_2 with NO to produce HNO_3 (R2b) must be accompanied by further slowing of the k_{1a} rate. In the air mass we are evaluating, HO_2 was constant to within 25% at 6.7×10^7 molecules/cm^3. If the k_{1a} rate were zero, than the measurements would give the k_{2b} of $1.9(\pm1.0)\times10^{-13}$ cm^3/molecules/s. If this were the case, we calculate a branching ratio of 1.7% for HNO_3 production in the HO_2 and NO reaction. On the other hand, if we assume the production by OH and NO_2 is 50% of the recommended value (~4.4×10^{-12} cm^3/molecules/s), then we find a branching ratio no larger than 0.8% for R2b. This is similar to the laboratory value.[11-13] For the R2b branching ratios in the range of 0 to 0.7%, we find k_{1a} ranges from $6.2(\pm2.9)$ – $4.7(\pm2.6)\times10^{-12}$ cm^3/molecules/s, respectively.

4.2 Speciated peroxy nitrate production

The observed production rates of PAN, PPN, $CH_3O_2NO_2$, and HO_2NO_2 versus NO_2 are shown in Fig. 7. The calculations to produce Fig. 7 are similar to the $HNO_{3,(g+p)}$ production and described in Sect. 4.2. Unlike HNO_3, we do not have observations of the respective radical species that produce the peroxy nitrates, except for HO_2NO_2. We use the observations (Table 1) to calculate the production rates of the respective radical species using the rate constants found in Table S1 – S3. For the case of PPN, we use the relationship observed by Singh et al.[49] between acetaldehyde and propanal to estimate propanal, which was not observed. Then, we use the calculated radical production rate and observed slopes from Fig. 7 to converge to a radical concentration and NO_2 rate constant. All the peroxy nitrate lifetimes are calculated to be longer than the length of the experiment (greater than 3 hours); therefore, their loss is not important to the assessment of the speciated peroxy nitrate production rate constants.

The calculated rate constants for the speciated peroxy nitrates are compared with the recommended rate constants in Table 2. The uncertainty in the rate constants, ranging from ~ 50 – ~75%, is defined by the uncertainty in the slopes and the spread in the radical concentrations (±25% for the inter-quartiles) or the uncertainty in the HO_2 concentration ($1\sigma \approx 16\%$).We find agreement (less than 30% difference) between the recommended[10] and calculated rate constants for the peroxy nitrates except for HO_2NO_2. Our calculated rate constants support the current recommendations[10] for the production rates of PAN, PPN, and $CH_3O_2NO_2$ for the conditions of the upper troposphere and the findings of Bacak et al.,[14] that the HO_2NO_2 production is slower than the recommendation by ~50%. The lower HO_2NO_2 is also consistent with the conclusions of Kim et al.,[33] that the current recommendations[10] produced more HO_2NO_2 than observed in the

upper troposphere. To our knowledge, this is the first time that the PAN and PPN production rates have been reported for the conditions representative of the upper troposphere.

4.3 Alkyl and multifunctional nitrate production

To evaluate the production of $\sum ANs_{(g+p)}$, we compare $\Sigma ANs_{(g+p)}$ and O_3 mixing ratios (Fig. 8a). As described by Perring et al.,[50] the slope of a plot of O_3 versus $\Sigma ANs_{(g+p)}$ is approximately equal to $2/\alpha$, where α is the ratio of $k_{3a}/(k_{3a} + k_{3b})$, as seen in Eq. 1 – 3. This assumes all the hydrocarbons oxidized produce two O_3 molecules ($\gamma = 2$).

$$P(O_3) = \sum_i \gamma_i (1 - \alpha_i) k_{OH+RH_i}[OH][RH_i] \quad (1)$$

$$P\left(\sum ANs_{(g+p)}\right) = \sum_i \alpha_i k_{OH+RH_i}[OH][RH_i] \quad (2)$$

$$P(O_3) = \frac{\bar{\gamma}(1-\bar{\alpha})}{\bar{\alpha}} P\left(\sum ANs_{(g+p)}\right) \approx \frac{2}{\bar{\alpha}} P\left(\sum ANs_{(g+p)}\right) \quad (3)$$

From the O_3 versus $\sum ANs_{(g+p)}$ correlation, we calculate an effective branching ratio, $\bar{\alpha}$, (1σ) of 8(±2)%.

For comparison, we calculate the $\Sigma ANs_{(g+p)}$ production rate directly using the temperature and pressure dependent parameterization of $\Sigma ANs_{(g+p)}$ formation from Carter and Atkinson[51] and the observations of the various hydrocarbons (Tables 1 and S4 and description of calculation in Supporting Information). Lee et al.[52] showed that at 273 K, $\Sigma ANs_{(g+p)}$ production is 50% more

efficient than at 300 K and even larger increases are calculated here for T = 225 K (250% more efficient). The direct calculation gives an average (1σ) $\bar{\alpha}$ of 7(±4)%. The uncertainty in $\bar{\alpha}$ includes uncertainty in the rate constants (~15%), the hydrocarbon concentrations (~10%), the OH concentration (~16%), and the temperature and pressure dependent α value (~30%). The calculated increase of ΣANs over the quasi-Lagrangian portion of the flight is (46(±18) pptv) (Fig. 8b).

In this air mass, the hydrocarbons that produce the largest fraction of the $\Sigma ANs_{(g+p)}$ (~70% or 34 pptv) are a group that have chemical lifetimes of less than 1 hour (MVK, MACR, isoprene, and monoterpene) and a group with longer lifetimes but still than 6 hours (greater than C6 hydrocarbons). These short lifetimes suggest that the $\Sigma ANs_{(g+p)}$ production rate will not be sustained downwind of lightning NO_x injection into the upper troposphere and only impacts the NO_x lifetime. Observations of $\Sigma ANs_{(g+p)}$ in the upper troposphere were typically ~90 pptv, which is a factor of 2 – 4 lower than the $\Sigma ANs_{(g+p)}$ mixing ratios in the outflow of convection, confirming that $\Sigma ANs_{(g+p)}$ production is primarily important in the near-field (Fig. 3c).

The multifunctional organic nitrates produced after radical isomerization or from biogenic hydrocarbons at the low temperatures of the upper troposphere are to have low vapor pressures and condense onto aerosol particles. During the flight, an apparent production rate of 2.2×10^{-3} $\mu g/m^3$ (at ambient T and P), or 3 pptv, $\Sigma ANs_{(p)}$ was observed (Fig. 9). We use the method described by Fry et al.[39] to differentiate between $NO_3^-{}_{(p)}$ and $\sum ANs_{(p)}$. This accounts for approximately 7% of the $\Sigma ANs_{(g+p)}$ observed during the flight.

We calculate the vapor pressures of the individual ΣANs using the SIMPOL.1 model[53] and the contribution to the aerosol phase using the equilibrium absorptive partitioning formalism[54] (Eq. 4 – 5 and Table S5). The largest contribution to the $\Sigma ANs_{(p)}$ are the

monoterpene hydroxy nitrates, isoprene dihydroxy dinitrates, and hydroxy nitrates formed from the isomerization of n-hexane, methyl hexanes, and n-heptane (Table S5). Explanation of the variables is found in Supporting Information.

$$K_p = \frac{R \cdot T \cdot f_{om}}{MW_{om} \cdot 10^6 \cdot \zeta \cdot p_{vap}} \quad (4)$$

$$m_{AN_{i,p}} = K_{p,i} \bullet m_{om} \bullet m_{AN_{i,g}} \quad (5)$$

The calculated $\Sigma ANs_{(p)}$ at the end of the experiment is 5.8×10^{-4} μg/m^3, which is a factor 4 lower than observations. Prior studies have concluded that the SIMPOL.1 model can overestimate the vapor pressures of multifunctional nitrates by up to 2 orders of magnitude, which is compounded by the need to estimate them at unusually low temperatures (225 K).[55-57] Given the prior discrepancy, a factor of 4 difference is not surprising. If the estimated vapor pressures are reduced by a factor of 3 (well within the uncertainties), then good model-measurement agreement is observed (Fig. 9).

5. Atmospheric Implications

Our results indicate that both the HNO_3 and HO_2NO_2 production rate are slower in the upper troposphere than in current models, consistent with recent reports.[19,33,58] Production of $\Sigma ANs_{(g+p)}$ depends on temperature and, as a result, is more rapid than in some current models. Production of $CH_3O_2NO_2$, PAN, and PPN are observed to occur at the rates currently recommended, although many models do not include $CH_3O_2NO_2$. Incorporating all of these changes and using the observations during the DC3 experiment to constrain a steady state model,

we find the NO_x lifetime increases by 20% (Fig. 10), leading up to as much as ~10 hour increases in the NO_x lifetime, and consequently, to higher O_3 production.

Some recent model studies have added the R2b yield without adjustment of the HNO_3 production rate.[59-61] Not surprisingly, these models result in too little NO_x and too much HNO_3 compared to observations. One study[19] decreased the HNO_3 production rate based on the recommendations from Henderson et al.,[48] who analyzed upper tropospheric NO_x observations from the Intercontinental Chemical Transport Experiment – North America, and the authors did not include R2b. The slower HNO_3 production rate decreased the HNO_3 concentrations by ~5 – 20 pptv and increased the NO_x concentrations by a similar amount. Bacak et al.[14] calculated the impact of the slower HO_2NO_2 production rate on HO_2NO_2 and NO_x. They report a decrease in HO_2NO_2 of 30 – 40% and an increase in NO_x of 5 – 20%.

To investigate the impacts of the slower HNO_3 and HO_2NO_2 production compared to current recommendations, we use GEOS-Chem v9-02b (details in Supporting Information) to model the year 2012 (Fig. 11). The largest NO_x increases (> 15 pptv for the entire year) occur over regions (central Africa, southeast United States, and northern India) of high lightning and deep convection.[62] The combined effects of slower HNO_3 and slower HO_2NO_2 production leads to larger changes in NO_x and O_3 concentrations than calculated with only a slower HNO_3 rate.[19] The increases in NO_x concentrations are associated with decreases in HNO_3 and HO_2NO_2 concentrations (up to 20 and 15 pptv, respectively) and increases in OH, PAN, $CH_3O_2NO_2$, and O_3 concentrations (up to 0.04, 15, and 5 pptv and 5 ppbv, respectively). HO_2 concentrations change little due to the competing effects of decreased HO_2NO_2 production and increased NO concentrations. The increases in both PAN and $CH_3O_2NO_2$ concentrations are associated with O_3

increases. The increased production of these less stable NO_z species allows transport of NO_x and leads to O_3 production downwind of the NO_x source.[63]

5. Conclusions

We have directly measured the production rates of speciated peroxy nitrates, alkyl and multifuctional nitrates, and HNO_3 in the upper troposphere. Using these observations to infer rate constants for the reactions at the temperature and pressure of the upper troposphere, we find that the rate of OH and NO_2 (k_{1a}) to produce HNO_3 is slower than currently recommended, making peroxy nitrate production as important as HNO_3 production as a sink of NO_x in the near field of lightning NO_x injection. The observations indicate that any HNO_3 production from the reaction of HO_2 with NO is small, which suggests the combined effects of k_{1a} and k_{2b} should not exceed the estimate for k_{1a} when k_{2b} is assumed to be zero. We also calculate that the HO_2NO_2 production rate is ~50% slower than currently recommended, supporting conclusions of Bacak et al.[14] We show that in the near field of deep convection, the effective average branching ratio to forming $\sum ANs_{(g+p)}$, $\bar{\alpha}$, is high (~8%) and dominated by short-lived hydrocarbons. Combining these ideas in a global chemical transport model, we demonstrate that decreases in the HNO_3 and HO_2NO_2 production rates lead to increases in the calculated upper tropospheric NO_x (10 – 14%), OH (10 – 13%), and O_3 (5 – 6%) concentrations.

Acknowledgements

BAN was supported by the National Science Foundation Graduate Research Fellowship under grant no. DGE 1106400. BAN, CG, PWJ, and RCC acknowledge funding support from NASA (NNX12AB79G). PTR-MS measurements aboard the NASA DC-8 were supported by the Austrian Federal Ministry for Transport, Innovation and Technology (bmvit) through the Austrian Space Applications Programme (ASAP) of the Austrian Research Promotion Agency (FFG). TM was supported by an appointment to the NASA Postdoctoral Program at the Langley Research Center, administered by Oak Ridge Associated Universities through a contract with NASA. JDC and POW acknowledge funding support from NASA (NNX12AC06G and NNX14AP46G). PCJ and JLJ acknowledge funding form NASA (NNX12AC03G and NNX15AH33A). BAN would like to thank Joshua L. Laughner in his assistance in setting up and running the GEOS-Chem model. The authors also want to thank the ground and flight crews of the DC-8 and the DC3 science team. Finally, the authors want to thank Donald Blake for the use of the whole air sampler measurements, and Glenn Diskin for the use of the CH_4 observations.

Supporting Information Available

Description of the instrument intercomparisons for HO_2NO_2, peroxy nitrates, and HNO_3 is included in Supporting Information S3, description of the calculation of alkyl and multifunctional nitrate production is included in Supporting Information S4, description of variables in Eq. 4 – 5 in Supporting Information S4 – S5, and description of the GEOS-Chem model is included in Supporting Information S5. A figure showing intercomparisons of observations is in Supporting Information S6, and of the intercomparison between photostationary steady state and NO_2 observations is in Supporting Information S7. The full

flight path of the DC-8 during the experiment is in Supporting Information S8. The time series of speciated peroxy nitrate observations is in Supporting Information S9. The first order decay of toluene and ethyne is shown in Supporting Information S10. Rate constants used to calculate peroxy and acyl peroxy radical concentrations is located in Supporting Information S11 – S12. Parent compounds, rate constant, initial concentrations, branching ratios, and classification of product for Fig. 8b are in Supporting Information S13. Parent compound, vapor pressure, percent contribution to aerosol particle, and percent contribution to calculate $\Sigma ANs_{(p)}$ is in Supporting Information S15. This material is available free of charge via the Internet at http://pubs.acs.org.

References

1. Myre, G.; Shindell, D.; Breon, F. -.; Collins, W.; Fuglestvedt, J.; Huang, J.; Koch, D.; Lamarque, J. -.; Lee, D.; Mendoza, B., et al. Anthropogenic and Natural Radiative Forcing. In *Climate Change 2013: The Physical Science Basis. Contribution of Working Group I to the Fifth Assessment Report of the Intergovernmental Panel on Climate Change*; Stocker, T. F., Qin, D., Plattner, G. -., Tignor, M., Allen, S. K., Boschung, J., Nauels, A., Xia, Y., Bex, V. and Midgley, P. M., Eds.; Cambridge University Press, Cambridge, United Kingdom and New York, NY, USA: 2013; pp 659.

2. Levy, H.; Moxim, W. J.; Klonecki, A. A.; Kasibhatla, P. S. Simulated Tropospheric NO_x: Its Evaluation, Global Distribution and Individual Source Contributions. *J. Geophys. Res.: Atmos.* **1999***, 104*, 26279-26306.

3. Bertram, T. H.; Perring, A. E.; Wooldridge, P. J.; Crounse, J. D.; Kwan, A. J.; Wennberg, P. O.; Scheuer, E.; Dibb, J.; Avery, M.; Sachse, G., et al. Direct Measurements of the Convective Recycling of the Upper Troposphere. *Science* **2007***, 315*, 816-820.

4. Hudman, R. C.; Jacob, D. J.; Turquety, S.; Leibensperger, E. M.; Murray, L. T.; Wu, S.; Gilliland, A. B.; Avery, M.; Bertram, T. H.; Brune, W., et al. Surface and Lightning Sources of Nitrogen Oxides Over the United States: Magnitudes, Chemical Evolution, and Outflow. *J. Geophys. Res.: Atmos.* **2007***, 112*, D12S05.

5. Liang, Q.; Rodriguez, J. M.; Douglass, A. R.; Crawford, J. H.; Olson, J. R.; Apel, E.; Bian, H.; Blake, D. R.; Brune, W.; Chin, M., et al. Reactive Nitrogen, Ozone and Ozone Production in

the Arctic Troposphere and the Impact of Stratosphere-Troposphere Exchange. *Atmos. Chem. Phys.* **2011***, 11*, 13181-13199.

6. Jacob, D. J.; Heikes, B. G.; Fan, S. M.; Logan, J. A.; Mauzerall, D. L.; Bradshaw, J. D.; Singh, H. B.; Gregory, G. L.; Talbot, R. W.; Blake, D. R., et al. Origin of Ozone and NO_x in the Tropical Troposphere: A Photochemical Analysis of Aircraft Observations Over the South Atlantic Basin. *J. Geophys. Res.: Atmos.* **1996***, 101*, 24235-24250.

7. Schultz, M.; Jacob, D.; Bradshaw, J.; Sandholm, S.; Dibb, J.; Talbot, R.; Singh, H. Chemical NO_x Budget in the Upper Troposphere Over the Tropical South Pacific. *J. Geophys. Res.: Atmos.* **2000***, 105*, 6669-6679.

8. Cooper, M.; Martin, R. V.; Sauvage, B.; Boone, C. D.; Walker, K. A.; Bernath, P. F.; McLinden, C. A.; Degenstein, D. A.; Volz-Thomas, A.; Wespes, C. Evaluation of ACE-FTS and OSIRIS Satellite Retrievals of Ozone and Nitric Acid in the Tropical Upper Troposphere: Application to Ozone Production Efficiency. *J. Geophys. Res.: Atmos.* **2011***, 116*, D12306.

9. Mollner, A. K.; Valluvadasan, S.; Feng, L.; Sprague, M. K.; Okumura, M.; Milligan, D. B.; Bloss, W. J.; Sander, S. P.; Martien, P. T.; Harley, R. A., et al. Rate of Gas Phase Association of Hydroxyl Radical and Nitrogen Dioxide. *Science* **2010***, 330*, 646-649.

10. Sander, S. P.; Abbatt, J. P. D.; Barker, J. R.; Burkholder, J. B.; Friedl, R. R.; Golden, D. M.; Huie, R. E.; Kolb, C. E.; Kurylo, M. J.; Moortgat, G. K., et al. Chemical Kinetics and Photochemical Data for use in Atmospheric Studies, Evaluation no. 17. *JPL Publication 10-6, Jet Propulsion Laboratory, Pasadena,* **2011**.

11. Butkovskaya, N. I.; Kukui, A.; Pouvesle, N.; Le Bras, G. Formation of Nitric Acid in the Gas-Phase HO_2 + NO Reaction: Effects of Temperature and Water Vapor. *J. Phys. Chem. A* **2005**, *109*, 6509-6520.

12. Butkovskaya, N.; Kukui, A.; Le Bras, G. HNO_3 Forming Channel of the HO_2 + NO Reaction as a Function of Pressure and Temperature in the Ranges of 72-600 Torr and 223-323 K. *J. Phys. Chem. A* **2007**, *111*, 9047-9053.

13. Butkovskaya, N.; Rayez, M.; Rayez, J.; Kukui, A.; Le Bras, G. Water Vapor Effect on the HNO_3 Yield in the HO_2 + NO Reaction: Experimental and Theoretical Evidence. *J. Phys. Chem. A* **2009**, *113*, 11327-11342.

14. Bacak, A.; Cooke, M. C.; Bardwell, M. W.; McGillen, M. R.; Archibald, A. T.; Huey, L. G.; Tanner, D.; Utembe, S. R.; Jenkin, M. E.; Derwent, R. G., et al. Kinetics of the HO_2 + NO_2 Reaction: On the Impact of New Gas-Phase Kinetic Data for the Formation of HO2NO2 on HOx, NO_x and HO_2NO_2 Levels in the Troposphere. *Atmos. Environ.* **2011**, *45*, 6414-6422.

15. Sander, S. P.; Peterson, M. E. Kinetics of the Reaction HO_2 + NO_2 + M → HO_2NO_2 + M. *J. Phys. Chem.* **1984**, *88*, 1566-1571.

16. Kurylo, M. J.; Ouellette, P. A. Rate Constants for the Reaction HO_2 + NO_2 + N_2 → HO_2NO_2 + N_2 - the Temperature-Dependence of the Falloff Parameters. *J. Phys. Chem.* **1987**, *91*, 3365-3368.

17. Christensen, L. E.; Okumura, M.; Sander, S. P.; Friedl, R. R.; Miller, C. E.; Sloan, J. J. Measurements of the Rate Constant of HO_2 + NO_2 + N_2 → HO_2NO_2 + N_2 using Near-Infrared

Wavelength-Modulation Spectroscopy and UV-Visible Absorption Spectroscopy. *J. Phys. Chem. A* **2004**, *108*, 80-91.

18. Bacak, A.; Bardwell, M.; Raventos-Duran, M.; Percival, C.; Hamer, P.; Shallcross, D. Kinetics of the CH_3O_2 + NO_2 Reaction: A Temperature and Pressure Dependence Study using Chemical Ionisation Mass Spectrometry. *Chem. Phys. Lett.* **2006**, *419*, 125-129.

19. Seltzer, K. M.; Vizuete, W.; Henderson, B. H. Evaluation of Updated Nitric Acid Chemistry on Ozone Precursors and Radiative Effects. *Atmos. Chem. Phys.* **2015**, *15*, 5973 - 5986.

20. Romps, D. M.; Seeley, J. T.; Vollaro, D.; Molinari, J. Climate Change. Projected Increase in Lightning Strikes in the United States due to Global Warming. *Science* **2014**, *346*, 851-854.

21. Barth, M. C.; Cantrell, C. A.; Brune, W. H.; Rutledge, S. A.; Crawford, J. H.; Huntrieser, H.; Carey, L. D.; MacGorman, D.; Weisman, M.; Pickering, K. E., et al. The Deep Convective Clouds and Chemistry (DC3) Field Campaign. *Bull. Am. Meteorol. Soc.* **2015**, *96*, 1281-1309.

22. National Aeronautical and Space Agency, Deep Convective Clouds and Chemistry, DC-8, Version 5. *10.5067/Aircraft/DC3/DC8/Aerosol-TraceGas* (accessed September 20, 2014).

23. Thornton, J. A.; Wooldridge, P. J.; Cohen, R. C. Atmospheric NO_2: In Situ Laser-Induced Fluorescence Detection at Parts Per Trillion Mixing Ratios. *Anal. Chem.* **2000**, *72*, 528-539.

24. Cleary, P. A.; Wooldridge, P. J.; Cohen, R. C. Laser-Induced Fluorescence Detection of Atmospheric NO_2 with a Commercial Diode Laser and a Supersonic Expansion. *Appl. Opt.* **2002**, *41*, 6950-6956.

25. Diskin, G. S.; Podolske, J. R.; Sachse, G. W.; Slate, T. A. Open-Path Airborne Tunable Diode Laser Hygrometer, in: Diode Lasers and Applications in Atmospheric Sensing, Edited by: Fried, A. *SPIE Proceedings* **2002***, 4817*, 196-204.

26. Browne, E. C.; Perring, A. E.; Wooldridge, P. J.; Apel, E.; Hall, S. R.; Huey, L. G.; Mao, J.; Spencer, K. M.; Clair, J. M. S.; Weinheimer, A. J., et al. Global and Regional Effects of the Photochemistry of $CH_3O_2NO_2$: Evidence from ARCTAS. *Atmos. Chem. Phys.* **2011***, 11*, 4209-4219.

27. Nault, B. A.; Garland, C.; Pusede, S. E.; Wooldridge, P. J.; Ullmann, K.; Hall, S. R.; Cohen, R. C. Measurements of $CH_3O_2NO_2$ in the Upper Troposphere. *Atmos. Meas. Tech.* **2015***, 8*, 987 - 997.

28. Wooldridge, P. J.; Perring, A. E.; Bertram, T. H.; Flocke, F. M.; Roberts, J. M.; Singh, H. B.; Huey, L. G.; Thornton, J. A.; Wolfe, G. M.; Murphy, J. G., et al. Total Peroxy Nitrates (ΣPNs) in the Atmosphere: The Thermal Dissociation-Laser Induced Fluorescence (TD-LIF) Technique and Comparisons to Speciated PAN Measurements. *Atmos. Meas. Tech.* **2010***, 3*, 593-607.

29. Day, D.; Wooldridge, P.; Dillon, M.; Thornton, J.; Cohen, R. A Thermal Dissociation Laser-Induced Fluorescence Instrument for in Situ Detection of NO_2, Peroxy Nitrates, Alkyl Nitrates, and HNO_3. *J. Geophys. Res.: Atmos.* **2002***, 107*, 4046.

30. Rollins, A. W.; Smith, J. D.; Wilson, K. R.; Cohen, R. C. Real Time in Situ Detection of Organic Nitrates in Atmospheric Aerosols. *Environ. Sci. Technol.* **2010***, 44*, 5540-5545.

31. Atkinson, R.; Baulch, D.; Cox, R.; Crowley, J.; Hampson, R.; Hynes, R.; Jenkin, M.; Rossi, M.; Troe, J. Evaluated Kinetic and Photochemical Data for Atmospheric Chemistry: Volume I - Gas Phase Reactions of O_x, HO_x, NO_x and SO_x Species. *Atmos. Chem. Phys.* **2004**, *4*, 1461-1738.

32. Atkinson, R.; Baulch, D. L.; Cox, R. A.; Crowley, J. N.; Hampson, R. F.; Hynes, R. G.; Jenkin, M. E.; Rossi, M. J.; Troe, J. Evaluated Kinetic and Photochemical Data for Atmospheric Chemistry: Volume II - Gas Phase Reactions of Organic Species. *Atmos. Chem. Phys.* **2006**, *6*, 3625-4055.

33. Kim, S.; Huey, L. G.; Stickel, R. E.; Tanner, D. J.; Crawford, J. H.; Olson, J. R.; Chen, G.; Brune, W. H.; Ren, X.; Lesher, R., et al. Measurement of HO_2NO_2 in the Free Troposphere during the Intercontinental Chemical Transport Experiment - North America 2004. *J. Geophys. Res.: Atmos.* **2007**, *112*, D12S01.

34. Ryerson, T.; Huey, L.; Knapp, K.; Neuman, J.; Parrish, D.; Sueper, D.; Fehsenfeld, F. Design and Initial Characterization of an Inlet for Gas-Phase NO_y Measurements from Aircraft. *J. Geophys. Res.: Atmos.* **1999**, *104*, 5483-5492.

35. Faloona, I.; Tan, D.; Lesher, R.; Hazen, N.; Frame, C.; Simpas, J.; Harder, H.; Martinez, M.; Di Carlo, P.; Ren, X., et al. A Laser-Induced Fluorescence Instrument for Detecting Tropospheric OH and HO_2: Characteristics and Calibration. *J. Atmos. Chem.* **2004**, *47*, 139-167.

36. Crounse, J. D.; McKinney, K. A.; Kwan, A. J.; Wennberg, P. O. Measurement of Gas-Phase Hydroperoxides by Chemical Ionization Mass Spectrometry. *Anal. Chem.* **2006***, 78*, 6726-6732.

37. St. Clair, J. M.; McCabe, D. C.; Crounse, J. D.; Steiner, U.; Wennberg, P. O. Chemical Ionization Tandem Mass Spectrometer for the in Situ Measurement of Methyl Hydrogen Peroxide. *Rev. Sci. Instrum.* **2010***, 81*, 094102.

38. DeCarlo, P. F.; Kimmel, J. R.; Trimborn, A.; Northway, M. J.; Jayne, J. T.; Aiken, A. C.; Gonin, M.; Fuhrer, K.; Horvath, T.; Docherty, K. S., et al. Field-Deployable, High-Resolution, Time-of-Flight Aerosol Mass Spectrometer. *Anal. Chem.* **2006***, 78*, 8281-8289.

39. Fry, J. L.; Draper, D. C.; Zarzana, K. J.; Campuzano-Jost, P.; Day, D. A.; Jimenez, J. L.; Brown, S. S.; Cohen, R. C.; Kaser, L.; Hansel, A., et al. Observations of Gas- and Aerosol-Phase Organic Nitrates at BEACHON-RoMBAS 2011. *Atmos. Chem. Phys.* **2013***, 13*, 8585-8605.

40. Talbot, R.; Dibb, J.; Lefer, B.; Scheuer, E.; Bradshaw, J.; Sandholm, S.; Smyth, S.; Blake, D.; Blake, N.; Sachse, G., et al. Large-Scale Distributions of Tropospheric Nitric, Formic, and Acetic Acids Over the Western Pacific Basin during Wintertime. *J. Geophys. Res.: Atmos.* **1997***, 102*, 28303-28313.

41. Blake, N. J.; Blake, D. R.; Simpson, I. J.; Meinardi, S.; Swanson, A. L.; Lopez, J. P.; Katzenstein, A. S.; Barletta, B.; Shirai, T.; Atlas, E., et al. NMHCs and Halocarbons in Asian Continental Outflow during the Transport and Chemical Evolution Over the Pacific

(TRACE-P) Field Campaign: Comparison with PEM-West B. *J. Geophys. Res.: Atmos.* **2003***, 108*, 8806.

42. Slusher, D. L.; Huey, L. G.; Tanner, D. J.; Flocke, F. M.; Roberts, J. M. A Thermal Dissociation-Chemical Ionization Mass Spectrometry (TD-CIMS) Technique for the Simultaneous Measurement of Peroxyacyl Nitrates and Dinitrogen Pentoxide. *J. Geophys. Res.: Atmos.* **2004***, 109*, D19315.

43. Wisthaler, A.; Hansel, A.; Dickerson, R. R.; Crutzen, P. J. Organic Trace Gas Measurements by PTR-MS during INDOEX 1999. *J. Geophys. Res.: Atmos.* **2002***, 107*, 8024.

44. Sachse, G. W.; Hill, G. F.; Wade, L. O.; Perry, M. G. Fast-Response, High-Precision Carbon Monoxide Sensor using a Tunable Diode Laser Absorption Technique. *J. Geophys. Res.: Atmos.* **1987***, 92*, 2071-2081.

45. Apel, E. C.; Olson, J. R.; Crawford, J. H.; Hornbrook, R. S.; Hills, A. J.; Cantrell, C. A.; Emmons, L. K.; Knapp, D. J.; Hall, S.; Mauldin III, R. L., et al. Impact of the Deep Convection of Isoprene and Other Reactive Trace Species on Radicals and Ozone in the Upper Troposphere. *Atmos. Chem. Phys.* **2012***, 12*, 1135-1150.

46. Bechara, J.; Borbon, A.; Jambert, C.; Colomb, A.; Perros, P. E. Evidence of the Impact of Deep Convection on Reactive Volatile Organic Compounds in the Upper Tropical Troposphere during the AMMA Experiment in West Africa. *Atmos. Chem. Phys.* **2010***, 10*, 10321-10334.

47. Atkinson, R. Kinetics and Mechanisms of the Gas-Phase Reactions of the Hydroxyl Radical with Organic-Compounds Under Atmospheric Conditions. *Chem. Rev.* **1986**, *86*, 69-201.

48. Henderson, B. H.; Pinder, R. W.; Crooks, J.; Cohen, R. C.; Carlton, A. G.; Pye, H. O. T.; Vizuete, W. Combining Bayesian Methods and Aircraft Observations to Constrain the $HO^{\cdot}$ + NO_2 Reaction Rate. *Atmos. Chem. Phys.* **2012**, *12*, 653-667.

49. Singh, H.; Salas, L.; Chatfield, R.; Czech, E.; Fried, A.; Walega, J.; Evans, M.; Field, B.; Jacob, D.; Blake, D., et al. Analysis of the Atmospheric Distribution, Sources, and Sinks of Oxygenated Volatile Organic Chemicals Based on Measurements Over the Pacific during TRACE-P. *J. Geophys. Res.: Atmos.* **2004**, *109*, D15S07.

50. Perring, A. E.; Pusede, S. E.; Cohen, R. C. An Observational Perspective on the Atmospheric Impacts of Alkyl and Multifunctional Nitrates on Ozone and Secondary Organic Aerosol. *Chem. Rev.* **2013**, *113*, 5848-5870.

51. Carter, W.; Atkinson, R. Alkyl Nitrate Formation from the Atmospheric Photooxidation of Alkanes - a Revised Estimation Method. *J. Atmos. Chem.* **1989**, *8*, 165-173.

52. Lee, L.; Wooldridge, P. J.; Gilman, J. B.; Warneke, C.; de Gouw, J.; Cohen, R. C. Low Temperatures Enhance Organic Nitrate Formation: Evidence from Observations in the 2012 Uintah Basin Winter Ozone Study. *Atmos. Chem. Phys.* **2014**, *14*, 12441-12454.

53. Pankow, J. F.; Asher, W. E. SIMPOL.1: A Simple Group Contribution Method for Predicting Vapor Pressures and Enthalpies of Vaporization of Multifunctional Organic Compounds. *Atmos. Chem. Phys.* **2008**, *8*, 2773-2796.

54. Pankow, J. F. An Absorption-Model of Gas-Particle Partitioning of Organic-Compounds in the Atmosphere. *Atmos. Environ.* **1994**, *28*, 185-188.

55. Fry, J. L.; Kiendler-Scharr, A.; Rollins, A. W.; Wooldridge, P. J.; Brown, S. S.; Fuchs, H.; Dubé, W. P.; Mensah, A.; dal Maso, M.; Tillmann, R., et al. Organic Nitrate and Secondary Organic Aerosol Yield from NO_3 Oxidation of Beta-Pinene Evaluated using a Gas-Phase Kinetics/Aerosol Partitioning Model. *Atmos. Chem. Phys.* **2009**, *9*, 1431-1449.

56. Fry, J. L.; Kiendler-Scharr, A.; Rollins, A. W.; Brauers, T.; Brown, S. S.; Dorn, H. -.; Dubé, W. P.; Fuchs, H.; Mensah, A.; Rohrer, F., et al. SOA from Limonene: Role of NO_3 in its Generation and Degradation. *Atmos. Chem. Phys.* **2011**, *11*, 3879-3894.

57. Leungsakul, S.; Jaoui, M.; Kamens, R. M. Kinetic Mechanism for Predicting Secondary Organic Aerosol Formation from the Reaction of D-Limonene with Ozone. *Environ. Sci. Technol.* **2005**, *39*, 9583-9594.

58. Henderson, B. H.; Pinder, R. W.; Crooks, J.; Cohen, R. C.; Hutzell, W. T.; Sarwar, G.; Goliff, W. S.; Stockwell, W. R.; Fahr, A.; Mathur, R., et al. Evaluation of Simulated Photochemical Partitioning of Oxidized Nitrogen in the Upper Troposphere. *Atmos. Chem. Phys.* **2011**, *11*, 275-291.

59. Cariolle, D.; Evans, M. J.; Chipperfield, M. P.; Butkovskaya, N.; Kukui, A.; Le Bras, G. Impact of the New HNO_3-Forming Channel of the HO_2 + NO Reaction on Tropospheric HNO_3, NO_x, HO_x and Ozone. *Atmos. Chem. Phys.* **2008**, *8*, 4061-4068.

60. Søvde, O. A.; Hoyle, C. R.; Myhre, G.; Isaksen, I. S. A. The HNO_3 Forming Branch of the HO_2 + NO Reaction: Pre-Industrial-to-Present Trends in Atmospheric Species and Radiative Forcings. *Atmos. Chem. Phys.* **2011***, 11*, 8929-8943.

61. Gottschaldt, K.; Voigt, C.; Joeckel, P.; Righi, M.; Deckert, R.; Dietmüller, S. Global Sensitivity of Aviation NO_x Effects to the HNO_3-Forming Channel of the HO_2 + NO Reaction. *Atmos. Chem. Phys.* **2013***, 13*, 3003-3025.

62. Miyazaki, K.; Eskes, H. J.; Sudo, K.; Zhang, C. Global Lightning NO_x Production Estimated by an Assimilation of Multiple Satellite Data Sets. *Atmos. Chem. Phys.* **2014***, 14*, 3277-3305.

63. Fischer, E. V.; Jacob, D. J.; Yantosca, R. M.; Sulprizio, M. P.; Millet, D. B.; Mao, J.; Paulot, F.; Singh, H. B.; Roiger, A.; Ries, L., et al. Atmospheric Peroxyacetyl Nitrate (PAN): A Global Budget and Source Attribution. *Atmos. Chem. Phys.* **2014***, 14*, 2679-2698.

64. Shetter, R. E.; Müller, M. Photolysis Frequency Measurements using Actinic Flux Spectroradiometry during the PEM-Tropics Mission: Instrumentation Description and some Results. *J. Geophys. Res.: Atmos.* **1999***, 104*, 5647-5661.

Table 1. Measurements used in this analysis to calculate rate constants, peroxy radical concentrations, average α, and ΣANs production rate.

Instrument	Species
Chemiluminescence[a]	NO, O_3
Thermal-Dissociation Laser-Induced Fluorescence[b]	NO_2, $CH_3O_2NO_2$, ΣPNs, $\Sigma ANs_{(g+p)}$
Laser-Induced Fluorescence[c]	OH, HO_2
Chemical Ionization-Mass Spectrometry[d]	$HNO_{3,g}$, CH_3OOH, $CH_3C(O)OOH$, Hydroxyacetone
Aerosol Mass Spectrometry[e]	$NO_3^-{}_{(p)}$, $\Sigma ANs_{(p)}$
Mist Chamber-Ion Chromatography[f]	$HNO_{3(g+p)}$
Chemical Ionization-Mass Spectrometry[g]	PAN, PPN, HO_2NO_2
Spectral Radiometry[h]	Photolysis Rates
Whole Air Sampler[i]	Hydrocarbons
Proton Transfer Reaction Mass Spectrometry[j]	Acetaldehyde, Acetone, Benzene, C8 Aromatics, Isoprene, Monoterpenes, MVK + MACR, Toluene
Tunable Diode Laser Absorption Spectroscopy[k]	CH_4

[a]Ref 34.

[b]Ref 23,27-30.

[c]Ref 35.

[d]Ref 36,37.

[e]Ref 38,39.

[f]Ref 40.

[g]Ref 33,42.

[h]Ref 64.

[i]Ref 41.

[J]Ref 43.

[k]Ref 25,44.

Table 2. Calculated and recommended rate constants (±2σ uncertainty) for speciated peroxy nitrates at T = 225 K and P = 230 hPa.[a]

Species	Calculated Rate Constant	Sander et al. Recommendations[b]	Recent Laboratory Results
PAN	$1.3(\pm0.8)\times10^{-11}$	$1.3^{+0.4}_{-0.3}\times10^{-11}$	N/A
PPN	$7.3(\pm3.4)\times10^{-12}$	$7.9^{+10.0}_{-4.4}\times10^{-12}$	N/A
$CH_3O_2NO_2$	$7.2(\pm5.7)\times10^{-12}$	$5.7^{+3.9}_{-2.3}\times10^{-12}$	$6.4(\pm0.5)\times10^{-12}$[c]
HO_2NO_2	$5.1(\pm3.1)\times10^{-13}$	$1.2^{+0.4}_{-0.3}\times10^{-12}$	$6.7^{+2.2}_{-1.7}\times10^{-13}$[d]

[a]Rate constants used to calculate the peroxy radical species are found in Tables S1 – S3.

[b]Ref 10.

[c]Ref 18. Rate is measured at 223 K and 267 hPa.

[d]Ref 14.

Figure Captions

Figure 1. Daytime NO_x fate in the upper troposphere. Reactions or channels that are not NO_x sinks (e.g., R2a) are not included. Double arrows indicate important thermal decomposition reactions that occur in the upper troposphere. Arrows and compounds in red (black) indicate reactions and products with NO (NO_2), and the blue arrow and reactants (products) in the bracket correspond to all the products. The lifetime for conversion back NO_x in the upper troposphere by photolysis and reactions with OH is days for all species except HO_2NO_2 and HOONO. For these two species, the lifetime is hours in the upper troposphere.

Figure 2. Portions of the NASA DC-8 flight path (blue) used to calculate all the rate constants. The wind direction and relative speed observed on the DC-8 for the 21 June 2012 flight is shown as red arrows. The edge of the cloud that marks time equals 0 for the Lagrangian observations is shown as the green dashed-dot line. Leg 1, 2, and 3 corresponds to the left most, center, and right most flight tracks.

Figure 3. Time series of **(a)** NO and NO_2, **(b)** ΣPNs_i, **(c)** $\Sigma ANs_{(g+p)}$, and **(d)** $HNO_{3(g+p)}$, where $\Sigma PNs_i = CH_3O_2NO_2 + HO_2NO_2 + PAN + PPN$ and $HNO_{3(g+p)}$ is the average of the IC and CIMS data. Note, NO_2 is blue and the left y-axis and NO is green and the right y-axis in **(a)**. Measurements not shown between 14:30 and 15:10 UTC are when the DC-8 sampled air outside the Lagragian parcel.

Figure 4. First order loss rate of ethene. The solid red line is the slope (-9.6×10^{-5} s^{-1}) and the dashed-dot red line is the 2σ uncertainty ($\pm1.4\times10^{-5}$ s^{-1}).

Figure 5. The observed $HNO_{3(g+p)}$ production rate (molecules/cm^3/s) versus NO_2 (molecules/cm^3). The solid red line is the slope (6.2×10^{-5} s^{-1}) and the dashed-dot line is the 2σ uncertainty ($\pm2.0\times10^{-5}$ s^{-1}).

Figure 6. Comparison of k_{1a} rate constant at T = 225 K and M = 7.3×10^{18} molecules/cm^3 from Sander et al.,[10] Atkinson et al.,[31] Henderson et al.,[48] and this study (red). The range shows the 2σ uncertainty of the product of the rate constant and branching ratio for HNO_3 formation.

Figure 7. The observed **(a)** PAN, **(b)** PPN, **(c)** $CH_3O_2NO_2$, and **(d)** HO_2NO_2 production rate (molecules/cm^3/s) versus NO_2 (molecules/cm^3). The solid red line is the slope and the dashed-dot red lines are the 2σ uncertainty. The slopes are **(a)** $4.5(\pm1.0)\times10^{-5}$ s^{-1}, **(b)** $6.8(\pm1.2)\times10^{-6}$ s^{-1}, **(c)** $8.4(\pm4.8)\times10^{-5}$ s^{-1}, and **(d)** $3.4(\pm1.8)\times10^{-5}$ s^{-1}. For **(c)**, three minute averages are used to reduce the noise of the measurements.

Figure 8. (a) The observed O_3 versus $\Sigma ANs_{(g+p)}$ during the flight. The slope (2σ uncertainty) is 25(±6). **(b)** The calculated cumulative production of alkyl and multifunctional nitrates (area plot in pptv) and the 15 minute average (±1σ of the mean) measured production (red error bars in pptv).

Figure 9. The observed (black at ambient T and P) and calculated (blue) cumulative production of the $\Sigma ANs_{(p)}$. The observations are 15 minute averages (±1σ of the spread) and the p_{vap} is reduced by a factor of 3.

Figure 10. Comparison of the NO_x lifetime (NO_x lifetime = NO_x/Loss of NO_z) in the upper troposphere (T ≤ 230 K) from a steady state model during the entire DC3 campaign. The base

case uses the recommended rate constants from Sander et al.,[10] and the updated chemistry case uses the rate constants from Henderson et al.[48] and Bacak et al.[14] The slope (±1σ) is 1.20(±0.01).

Figure 11. The absolute annual mean change in **(a)** NO_x, **(b)** HO_2, **(c)** OH, **(d)** O_3, **(e)** HNO_3, **(f)** PAN, **(g)** HO_2NO_2, and **(h)** $CH_3O_2NO_2$ in the upper troposphere (200 – 400 hPa). The mean change is calculated as (updated chemistry case – base case). Values above the tropopause are removed. Note the different scales for the color bars.

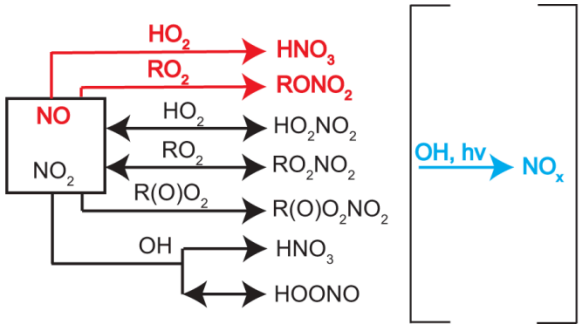
HO2
HNO3
RO2
RONO2
NO
HO2
HO2NO2
NO2
RO2
RO2NO2
R(O)O2
R(O)O2NO2
OH
HNO3
HOONO
OH, hv
NOx

Figure 1.

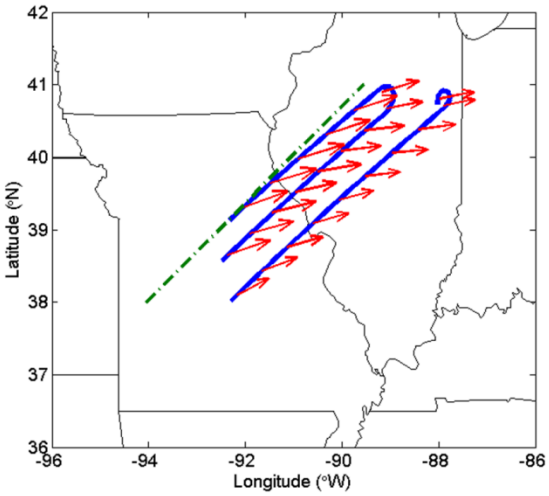

Figure 2.

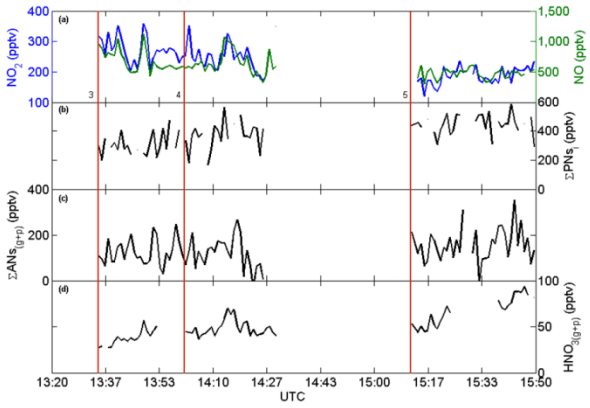
(a)
(b)
(c)
(d)
NO2 (pptv)
NO (pptv)
ΣPNs1 (pptv)
ΣANs(i+n) (pptv)
HNO3(i+n) (pptv)
3
4
5
13:20
13:37
13:53
14:10
14:27
14:43
15:00
15:17
15:33
15:50
UTC

Figure 3.

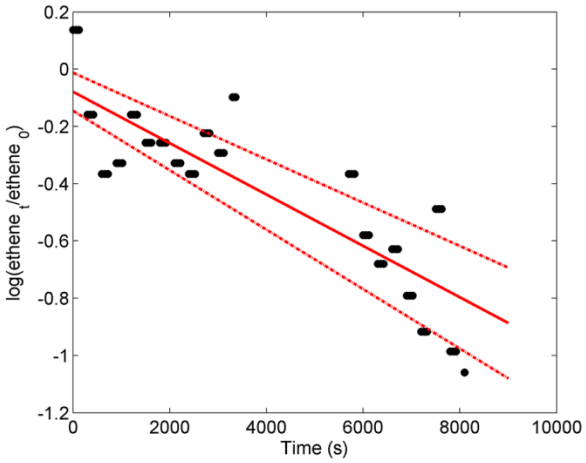
0.2
0
-0.2
-0.4
-0.6
-0.8
-1
-1.2
log(ethene t/ethene 0)
0
2000
4000
6000
8000
10000
Time (s)

Figure 4.

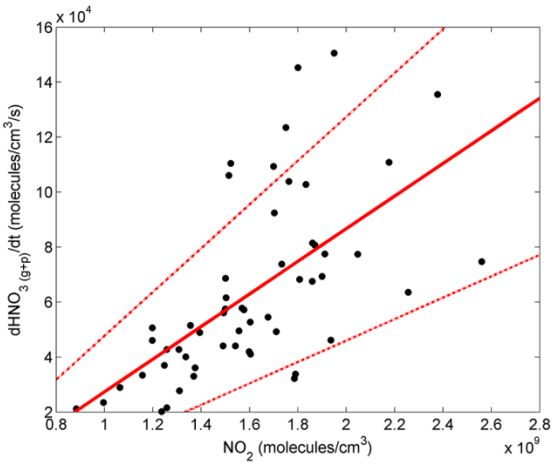
x 10^4
16
14
12
10
8
6
4
2
dHNO3 (g+p) /dt (molecules/cm3/s)
0.8
1
1.2
1.4
1.6
1.8
2
2.2
2.4
2.6
2.8
NO2 (molecules/cm3)
x 10^9

Figure 5.

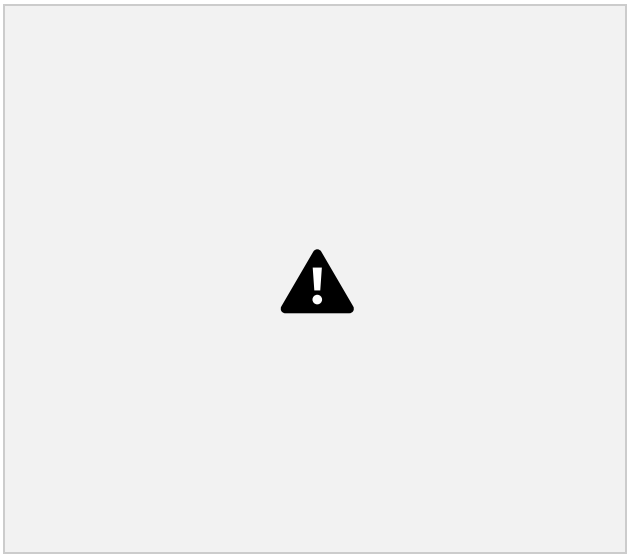

Figure 6.

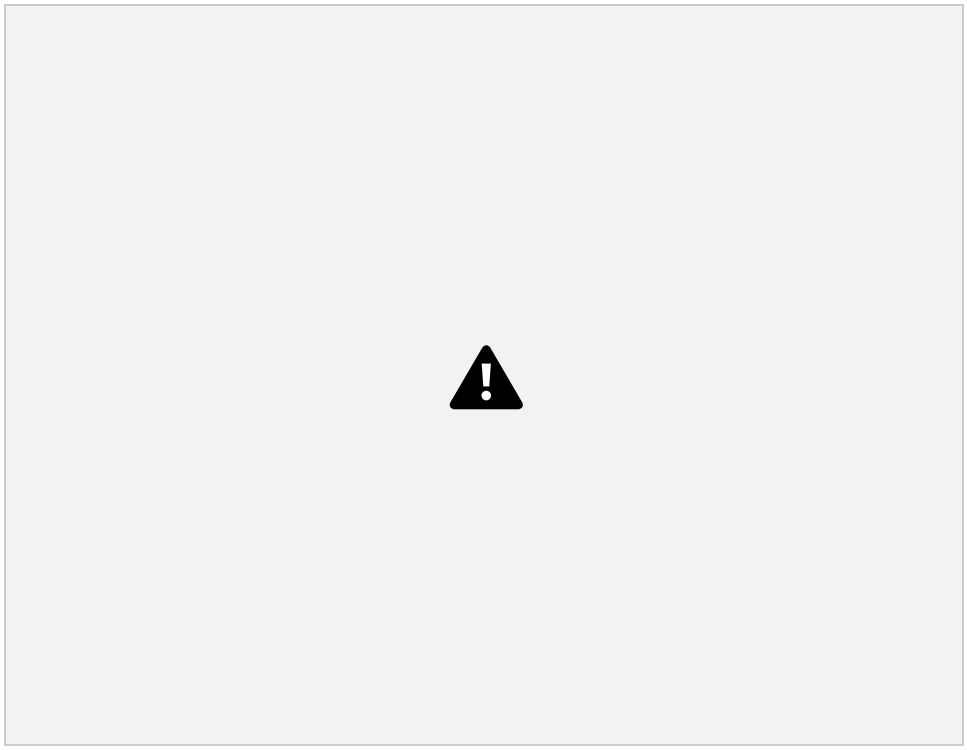

Figure 7.

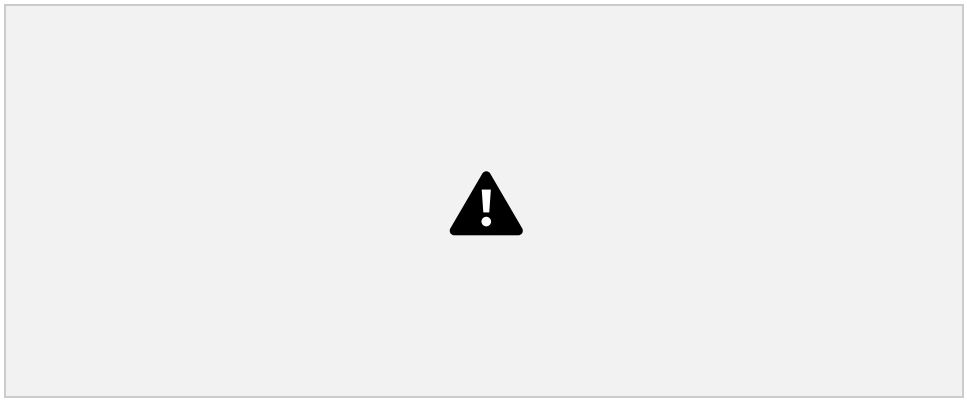

Figure 8.

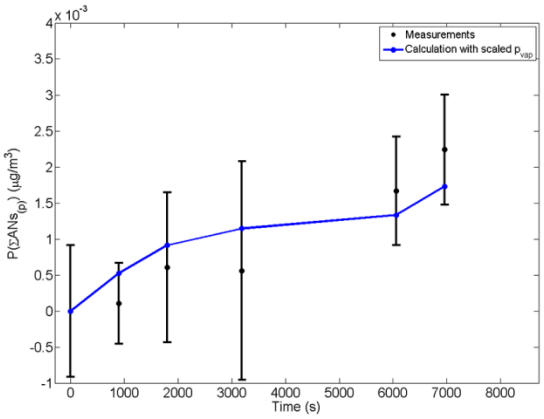
x 10^-3
Measurements
Calculation with scaled p_vap
P(ΣANS_(p)) (μg/m^3)
Time (s)
4
3.5
3
2.5
2
1.5
1
0.5
0
-0.5
-1
0
1000
2000
3000
4000
5000
6000
7000
8000

Figure 9.

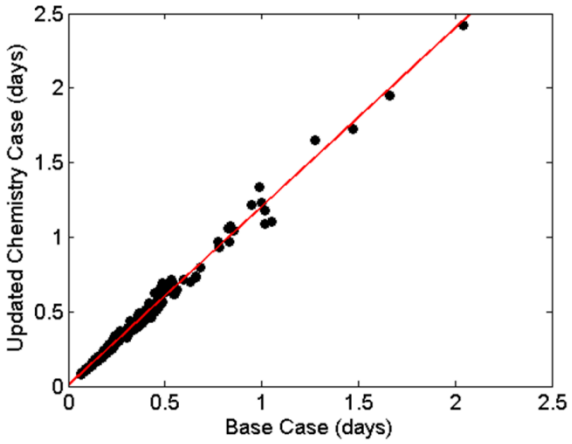

Figure 10.

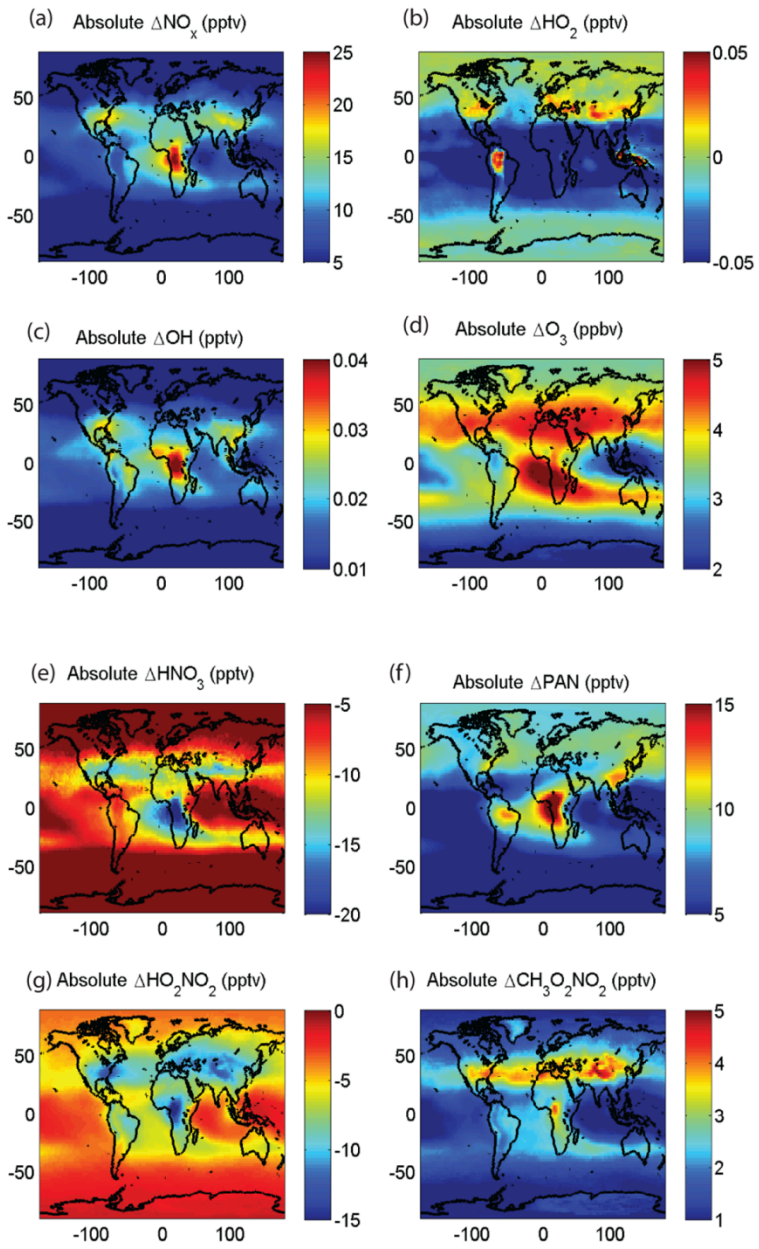
(a) Absolute ΔNOx (pptv)
(b) Absolute ΔHO2 (pptv)
(c) Absolute ΔOH (pptv)
(d) Absolute ΔO3 (ppbv)
(e) Absolute ΔHNO3 (pptv)
(f) Absolute ΔPAN (pptv)
(g) Absolute ΔHO2NO2 (pptv)
(h) Absolute ΔCH3O2NO2 (pptv)
50
0
-50
-100
0
100
25
20
15
10
5
0.05
0
-0.05
0.04
0.03
0.02
0.01
4
3
2
-5
-10
-15
-20
1

Figure 11.

Table of Contents Image